



Clay minerals trap hydrogen in the Earth's crust: Evidence from the Cigar Lake uranium deposit, Athabasca

Laurent Truche ^{a,b,*}, Gilles Joubert ^c, Maxime Dargent ^b, Pierre Martz ^b, Michel Cathelineau ^b, Thomas Rigaudier ^d, David Quirt ^e

^a Université Grenoble Alpes, CNRS, ISterre, F-38000 Grenoble, France

^b Université de Lorraine, CNRS, CREGU, GeoRessources, UMR 7359, BP 70239, F-54506 Vandoeuvre-lès-Nancy, France

^c Orano Mining BU, 1 place Jean Millier, F-92084 Paris La Défense Cedex, France

^d Université de Lorraine, CRPG UMR 7358 CNRS-UL, Vandoeuvre-lès-Nancy cedex, France

^e Orano Canada Inc., P.O. Box 9204, 810 - 45th Street West, Saskatoon, SK S7K 3X5, Canada

ARTICLE INFO

Article history:

Received 12 January 2018

Received in revised form 8 March 2018

Accepted 18 April 2018

Available online 3 May 2018

Editor: M. Bickle

Keywords:

hydrogen
sorption
clay
radiolysis
uranium deposit
storage

ABSTRACT

Hydrogen (H_2)-rich fluids are observed in a wide variety of geologic settings including gas seeps in serpentized ultramafic rocks, sub-seafloor hydrothermal vents, fracture networks in crystalline rocks from continental and oceanic crust, and volcanic gases. Natural hydrogen sources can sustain deep microbial ecosystems, induce abiotic hydrocarbons synthesis and trigger the formation of prebiotic organic compounds. However, due to its extreme mobility and small size, hydrogen is not easily trapped in the crust. If not rapidly consumed by redox reactions mediated by bacteria or suitable mineral catalysts it diffuses through the rocks and migrates toward the surface. Therefore, H_2 is not supposed to accumulate in the crust. We challenge this view by demonstrating that significant amount of H_2 may be adsorbed by clay minerals and remain trapped beneath the surface. Here, we report for the first time H_2 content in clay-rich rocks, mainly composed of illite, chlorite, and kaolinite from the Cigar Lake uranium ore deposit (northern Saskatchewan, Canada). Thermal desorption measurements reveal that H_2 is enriched up to 500 ppm (i.e. 0.25 mol kg^{-1} of rock) in these water-saturated rocks having a very low total organic content (<0.5 wt%). Such hydrogen uptake is comparable and even exceeds adsorbed methane capacities reported elsewhere for pure clay minerals or shales. Sudoite (Al-Mg di-trioctahedral chlorite) is probably the main mineral responsible for H_2 adsorption in the present case. The presence of multiple binding sites in interlinked nanopores between crystal layers of illite-chlorite particles offers the ideal conditions for hydrogen sorption. We demonstrate that 4 to 17% of H_2 produced by water radiolysis over the 1.4-Ga-lifetime of the Cigar Lake uranium ore deposit has been trapped in the surrounding clay alteration haloes. As a result, sorption processes on layered silicates must not be overlooked as they may exert an important control on the fate and mobility of H_2 in the crust. Furthermore, the high capacity of clay minerals to sorb molecular hydrogen may also open up new opportunities for exploration of unexpected energy resources and for H_2 storage based on geo-inspired materials.

© 2018 Elsevier B.V. All rights reserved.

1. Introduction

In the Earth's crust, hydrogen (H_2) concentration results from a complex balance between the deep mantle source input, the crustal production and consumption and the transport mechanisms of the molecule such as liquid/vapor partitioning, diffusion and advection. Besides being continuously released from the mantle, hydrogen is formed in the crust as a product of the hydration of ultramafic or peralkaline rocks (e.g. Neal and Stanger, 1983;

Charlou et al., 2002; Mayhew et al., 2013; Potter et al., 2013), by water radiolysis (Dubessy et al., 1988; Lin et al., 2005), as well as by some thermophilic bacteria (Huber et al., 1986; Hoehler et al., 2001). A portion of the produced H_2 is consumed either by lithospheric chemotrophes using H_2 for energy (Nealson et al., 2005; Sherwood Lollar et al., 2007), or by thermochemical redox reactions such as carbonate or sulfate reduction (e.g. Horita and Berndt, 1999; McCollom and Seewald, 2001; Proskurowski et al., 2008; Truche et al., 2009). The remaining is supposed to be vented in the oceans or the atmosphere. It is also possible that a large part of H_2 produced is retained beneath the subsurface and remains adsorbed at the surface of minerals. This potential sink or

* Corresponding author.

E-mail address: laurent.truche@univ-grenoble-alpes.fr (L. Truche).

reservoir is currently ignored in the H₂ budget and distribution in the crust (Cannat et al., 2010; Sherwood Lollar et al., 2014; Worman et al., 2016). Few laboratory experimental studies seem to indicate that hydrogen physisorption is feasible at the surface of clay minerals (Gil et al., 2009; Didier et al., 2012; Edge et al., 2014; Mondelli et al., 2015). However, the conditions (cryogenic temperature, dry and outgassed samples, pure synthetic swelling clays) used in these experiments are not representative of geologic settings complicating any attempts at extrapolation.

Here, we report hydrogen concentration in the mineralized area and in the clay alteration halo surrounding the Cigar Lake uranium orebody. The massive and focused presence of UO₂ led to pore water radiolysis and therefore to a localized H₂ production (Liu and Neretnieks, 1996; Bruno and Spahiu, 2014). The simple lens-shaped geometry of the deposit (2200 m long, by 25–100 m wide, by 1–20 m high) and its depth (~430 m), which precludes effects from recent weathering and erosion, provide a unique opportunity to study hydrogen behavior in sedimentary and basement rocks. Results provide clear evidence for hydrogen adsorption at the surface of clay minerals, and show that this process is far from being negligible in controlling hydrogen fate and mobility in the crust.

2. Geological setting

The Cigar Lake U deposit is located at the eastern rim of the Athabasca Basin (Saskatchewan province, Canada) at the unconformity between the sandstones of the Manitou Falls formation and the Aphebian metasediment basement known as the Wollaston Group (Bruneton, 1993). It is one of the many unconformity type sandstone-hosted U deposits of Proterozoic age that characterize the Athabasca Basin uranium province (Jefferson et al., 2007). The deposit was formed around 1.4–1.5 Ga (1461 ± 47 Ma) ago by hydrothermal processes, but several remobilizing events occurred especially within the range 300–400 Ma (Fayek et al., 2002). The massive and extremely focused uranium mineralization is mainly uraninite and pitchblende UO_{2+x}(s) with some subordinate coffinite. Total estimate reserves at Cigar Lake are 601,800 tons of ore at average U grade of 14.2 wt%, with local concentration reaching values as high as 60 wt% (Scott Bishop et al., 2016). The deposit is characterized by a series of alteration haloes geometrically arranged around the orebody, decreasing in intensity with increasing distance from the ore surface. The haloes comprise a massive clay zone of varying thickness (up to 30 m) immediately surrounding the orebody and mostly derived from the hydrothermal alteration of the sandstones, conglomerates, and basement rocks. The clay matrix directly associated with the high-grade mineralization consists of illite and sudoite (di-trioctahedral Al-Mg-chlorite) changing upward and outward to illite and kaolinite in the sandstones (Percival and Kodama, 1989; Percival et al., 1993; Billault et al., 2002). In the basement, the illite–sudoite clay assemblage is superimposed to the initial metamorphic muscovite and Fe–Mg trioctahedral chlorite. The massive orebody is almost exclusively sandstone-hosted and has sharp contacts with the highly argillitized basement below. Right above the orebody, a 5 m thick ferric rich illite–hematite–siderite rim occurs.

3. Materials and methods

3.1. Petrographic, mineralogical and textural analysis

The core samples were collected during a drilling campaign carried out by Cameco Corporation in 2014. Their exact location is reported in Table 1. Rock samples were characterized by microscopic observations under reflected light and by scanning electron microscopy (SEM). Unoriented bulk powders and oriented clay aggregates were characterized by X-ray diffraction using a D8 Bruker

diffractometer (Co K α , 40 kV, 40 mA). The clay mineral fraction (<2 μm) was extracted from samples by application of the Stoke's law and deposited on glass slides, which were analyzed three different ways: i) oriented clay mineral fraction, ii) ethylene glycol saturated, and iii) heated at 550 °C during 4 h. Each diffractogram was measured in the 2-θ domain. Whole-rock samples were analyzed for Fe and U concentration by ICP-OES.

The specific areas of the rock samples were obtained using the BET method on a Belsorp-Max apparatus using a cross sectional area on nitrogen (0.163 nm²). Solids were outgassed overnight at 150 °C down to a 3.0 × 10⁻⁵ Pa before analysis with N₂ at 77 K. The presence of micropores in the sample was checked using the t-plot method. Pore size distributions were calculated following the BJH method by applying the Non-Local Density Functional Theory (NLDFT) method.

3.2. Thermal desorption analysis

Core samples were packed and sealed in gas tight double liner plastic-alumina bags of 3 to 5 kg immediately after being recovered at the surface. In order to make sure that no hydrogen was released during storage, the gas phase present in the bags was sampled before opening thanks to a syringe and analyzed by gas chromatography (GC). Hydrogen was never found in detectable amount (<5 ppmv) in these hermetic envelopes. Then, the rock samples were split in two aliquots: one was loaded without any pre-processing in a 500 mL inox Parr® flow-through autoclave for thermal desorption run and the other one was crushed (<2 mm, agate mortar) and dried for 48 h at 40 °C before the desorption run in order to remove free bulk water, while avoiding gas desorption. Once loaded with a known amount of sample (~250 g), the autoclave was flushed with argon to avoid oxidation in the presence of air, and heated up to 600 °C by step of 20 to 50 °C. The duration of each temperature step was ~10 h, but longer steps (up to four days) were also tested to ensure the completeness of the desorption process at a given T. The autoclave was constantly flushed by argon at a flow rate of 0.1 l min⁻¹. The composition of the effluent gas was measured online by GC (Agilent® 490 Micro GC dual equipped with a 10 m Molecular Sieve 5A column and a 40 cm HayeSep A column) for H₂, He, N₂, CH₄, CO₂, and CO. The absolute concentration was calibrated to the area of the H₂, He, CH₄, and CO₂ peaks for standard gases. The estimated uncertainty in gas measurement is about 5%.

Batch thermal desorption runs were also performed (300 and 600 °C, 48 h, Ar) for comparison with the flow-through ones and bulk H₂ isotopic measurements. Hydrogen, recovered after these runs, was first purified in a vacuum glass line. H₂O, and CO₂ were trapped cryogenically with liquid nitrogen. Hydrogen was transferred into a special vessel with a septum using a Toeppler pump. Hydrogen isotopic composition was measured by injecting 500 μL of headspace gas into a modified EA-IRMS (isotopic ratio mass spectrometry) system equipped with a 1 m Molecular Sieve 5A methane separation column in line with a GV Isoprime IRMS. Hydrogen isotopic composition was expressed as δD value with a reference to Vienna standard mean ocean water (V-SMOW):

$$\delta D_{\text{‰}} = [(D/H)_{\text{sample}}/(D/H)_{\text{standard}} - 1] \times 1000 \quad (1)$$

where D is deuterium, and the standard is V-SMOW. Total error incorporating both accuracy and reproducibility is ±10‰ with respect to V-SMOW.

Table 1

Total amount of gases (H_2 , CH_4 and CO_2 – ppm = g per ton of rock) recovered by thermal desorption, uranium content and clay mineralogy of the Cigar Lake core samples investigated in this study.

#Borehole	UTM easting	UTM northing	Depth (m)	Grade wt% U	Desorption data (ppm)			<2 μ fraction – XRD data (wt%)			Surface area ($\text{m}^2 \text{g}^{-1}$)
					[H_2] (δD V-SMOW ‰)	[CO_2]	[CH_4]	Illite	Chlorite	Kaolinite	
SF-910-02	527386.89	6436710.7	431.3	0	0	53	0	nd	nd	nd	14.0
			444.1	0.03	12	343	17	75	25	0	
			448.3	0	7	111	0	nd	nd	nd	
SF-731-05	527272.79	6436724	417.1	nd	0	0	0	nd	nd	nd	14.0
			427.1	nd	5	0	0	nd	nd	nd	
			431	nd	20	9.2	0	71	0	29	
			432	4.5	58	1821	7	nd	nd	nd	
			433	5.7	86 (–552‰)	1073	6	58	0	42	
			435	20.9	254 (–582‰)	718	30	nd	nd	nd	
			449.7	nd	nd	nd	nd	60	40	0	
			450.4	nd	5	0	0	64	36	0	
			452.1	nd	8	0	0	71	29	0	
			454	nd	nd	nd	nd	66	34	0	
			454.7	nd	nd	nd	nd	81	20	0	
			456.4	nd	9	0	0	73	28	0	
			456.6	nd	nd	nd	nd	68	32	0	
			459.3	nd	nd	nd	nd	61	39	0	
			461	nd	nd	nd	nd	61	39	0	
SF-737-05	527278.598	6436740.096	438	nd	341	192	24	nd	nd	nd	
SF-910-07	527386.79	6436740.3	409.3	0	0	0	0	97	0	3	14.2
			416.5	0.01	0	0	0	99	0	1	
			423.2	0.04	25	1700	0	88	0	12	
			425.6	0.03	331 (–311‰)	23200	0	75	0	25	
			429.8	0.12	1119	76400	0	59	0	41	
			432.7	3.8	492	0	0	nd	nd	nd	
			433.3	8.6	357 (–557‰)	1000	0	nd	nd	nd	
			434.8	31.9	151	0	0	86	14	0	
			438.5	15.3	55	0	0	nd	nd	nd	
			439.7	1.9	54	0	0	75	25	0	
			442.3	0.9	195 (–517‰)	0	0	47	53	nd	
			445.2	0.07	101	600	0	nd	nd	nd	
			452.8	0	7	0	0	80	20	0	
			461	0	10	0	0	80	20	0	
SF-902-08	527386.85	6436748.5	425.2	0.36	17	995	0	75	25	0	19.3
SF-910-10	527386.54	6436758.5	440	0.09	172 (–542‰)	127	0	75	25	0	22.5
			441.6	0.81	112	60	0	47	53	0	
			391.7	0.01	0	57	0	nd	nd	nd	
			405.8	0.01	0	94	0	100	0	0	
			416.6	0.03	0	108	0	97	0	3	
			419	0.33	0	397	0	97	0	3	
			421.3	0.03	0	333	0	95	0	5	
			436.5	0.08	31	144	0	83	17	0	
			445.7	0	nd	nd	nd	87	13	0	
			452	0.01	0	43	0	61	39	0	
			459	0	4	86	0	75	25	0	
ST-896-12	527386.63	6436772.4	407.8	0.04	0	75	0	nd	nd	nd	
ST-900-15	527386.68	6436790.4	410.1	0.04	0	76	0	nd	nd	nd	18.0
			425.7	0	nd	nd	nd	84	0	16	
			443.8	0.01	0	74	0	nd	nd	nd	
			461.5	0	0	125	0	nd	nd	nd	
			439.7	0	20	73	0	75	25	0	
SF-910-18	527386.86	6436806.1	446.1	0	0	534	0	60	40	0	14.0
			455.5	0	0	144	0	82	18	0	
			461.2	0	nd	nd	nd	67	33	0	
			422.5	0.01	0	165	0	98	2	0	
			441.6	0.02	5	80	0	46	55	0	
			441.9	0.01	nd	nd	nd	84	16	0	
			446	0.01	5	131	0	41	59	0	
			447.8	0.02	nd	nd	nd	68	32	0	
			452.7	0	0	579	0	73	27	0	
			458.7	0	nd	nd	nd	46	54	0	

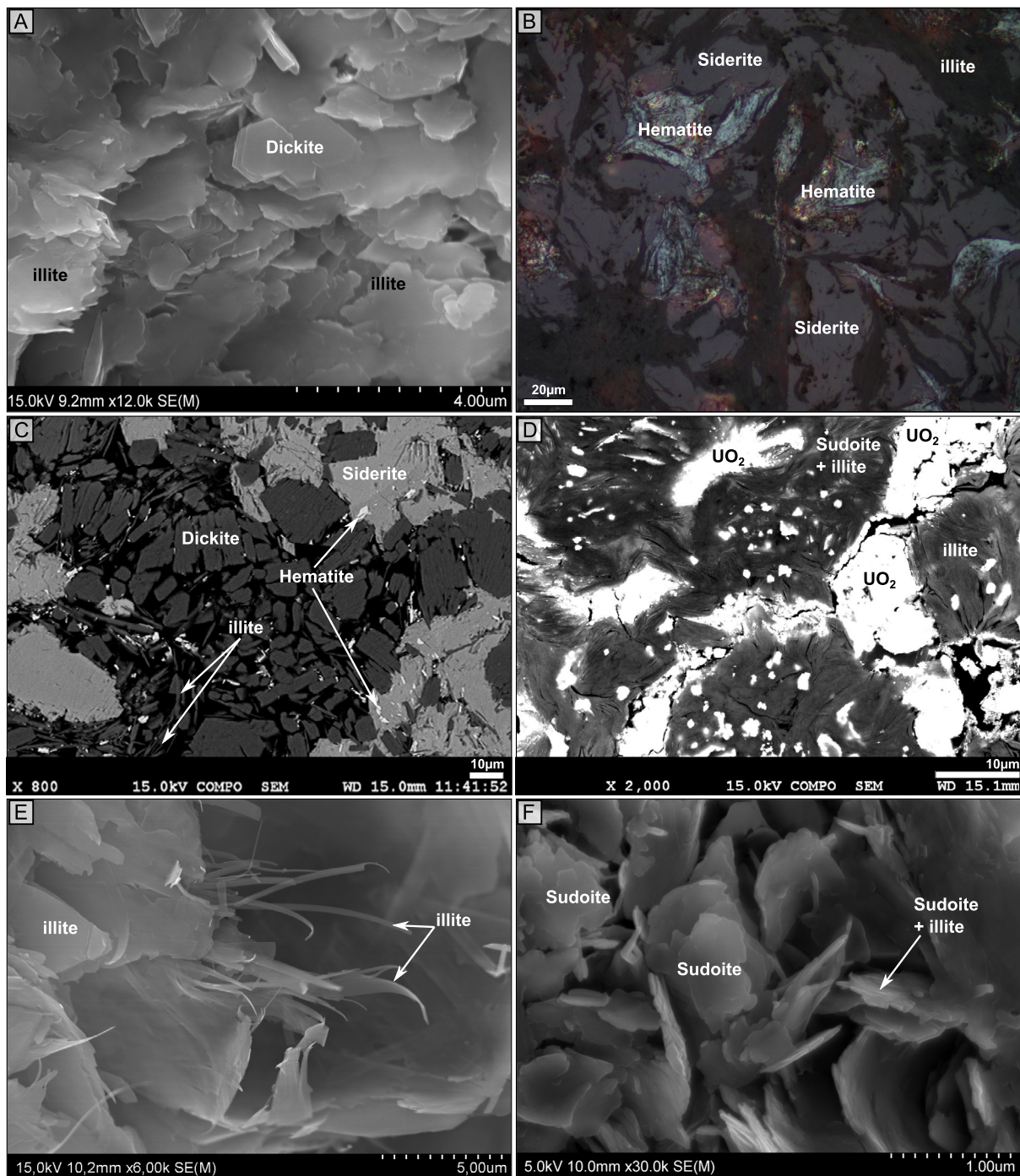


Fig. 1. Pictures of the distinct clay assemblages observed along borehole SF-910-07 in the Cigar Lake U deposit. (A) SEM picture of aggregates of pseudomorphic dickite platelets after kaolinite resembling books slightly destabilized by platy illite crystals (423.2 m). (B) Microscopic picture under reflected light of siderite crystals partially converted into hematite and embedded in an illite dominant clay matrix (429.8 m). (C) SEM picture of siderite crystals in a matrix dominated by dickite +/- platy illite crystals (429.8 m). (D) SEM picture of a close association of uranium oxides embedded in an intimately mixed illite and sudoite clay assemblage (434.8 m). (E) Zoomed SEM picture showing both coarse and thin hairy-like illite crystals (439.7 m). (F) SEM picture of a mechanical mixture of irregular sudoite flakes and platy illite crystals (442.3 m). (For interpretation of the colors in the figure(s), the reader is referred to the web version of this article.)

4. Results

4.1. Clay mineralogy of the Cigar Lake core samples

A total of 60 core samples from the different lithologies were collected from a series of nine vertical diamond drilled boreholes cross-cutting the whole orebody to a depth of 462 m. The different lithologies and their respective clay mineralogy (Table 1) are characterized as follow from the top to bottom:

- Several tens of meters above the deposit, the sandstones consist of more than 90% of sub-rounded to rounded detrital quartz with very minor detrital K-feldspar and plagioclase. The clay matrix is dominated by illite minerals replacing the diagenetic dickite (Fig. 1a) and forming an alteration halo extending to at least more than 100 m above the unconformity. In this halo, the diagenetic widespread iron oxides have been dissolved. Together with the dominant illite minerals, it gives a grey-whitish color to the sandstones. In addition, diagenetic

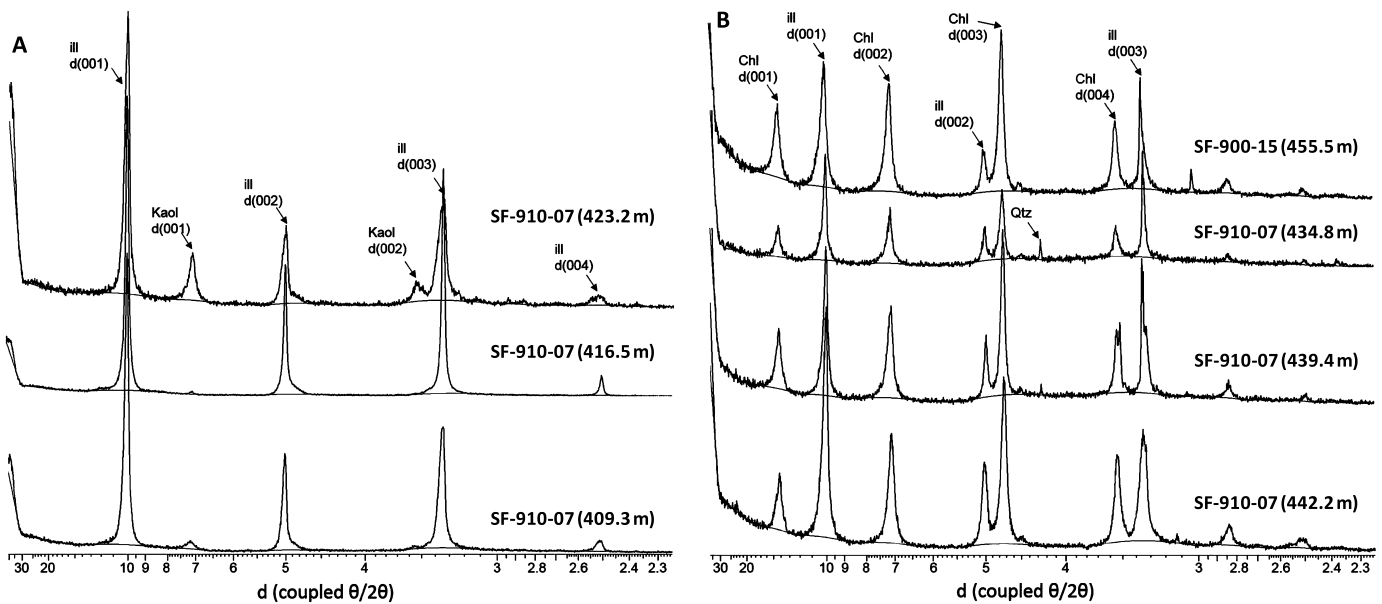


Fig. 2. X-ray-diffraction patterns (Co K α ; air-dried, oriented mounts) for samples located above the mineralization in the argillized sandstones (A), and in the argillized basement below the ore zone (B). III = illite, Kaol = kaolinite, Chl = chlorite, and Qtz = quartz. See Table 1 for samples location.

quartz overgrowths, highlighted by dustlines and small iron oxide crystals, show evidence of corrosion in the halo, indicating that diagenetic quartz cementation has been interrupted by at least one episode of quartz dissolution synchronous to the illite alteration. Latter euhedral quartz infilling fractures are common in the halo.

- As we move toward the orebody, in the 5 to 30 m above it, the sandstones become less competent, features of quartz dissolution become more and more intense and the clay matrix consists of 70% (locally 100%) of the total rock mineralogy. In this area, the uranium grade can go up to 0.2 wt% U. The intensity of the alteration increases toward the mineralization. Localized oxidized areas are common. The XRD patterns of oriented mounts of clay material indicate that the samples contain mostly illite with no expandable layers, but the kaolinite content increases toward the ore zone (Fig. 2a). The illite crystals (Fig. 1a and 1e) can be either coarse-grained and lath-shaped (cv-1M polytype) or thin and showing a hairy-like texture with elongated particles up to 1 μ m wide and a few tens of micrometers long (tv-1M polytype).
- Right above the main orebody, a hematitic clay-rich sandstone forms a ~5 m thick rim located at the interface between the grey altered sandstones and the ore. This sharp interface is red-brown to red-green in color. This zone is mostly composed of clay (up to 70 wt%) with strong features of quartz dissolution. Illite remains the dominant clay mineral in this area but kaolinite may represent 20 to 40% of the total clay content. Hematite represents up to 11 wt% of the rock giving an overall red color. Siderite can be locally abundant (up to 17 wt%) either as aggregate or euhedral crystals or as irregular layers and veins. The clays are generally weakly mineralized (0.01 to 0.2 wt% U), but local concentrations of up to several percent U are present. Hematite is found to replace siderite (Fig. 1b and 1c).
- The uranium mineralization has sharp contacts with the upper clay zone and the highly argillized basement. The massive ore lies right above the unconformity and may locally grade up to 60 wt% U. The mineralization occurs in a clay rich matrix dominated by illite and sudoite. Sudoite occurs as interlayered with illite or intimately linked with illite at a nanoscale (Fig. 1d).

The basement rocks located at least 20 m below the unconformity are strongly altered and all the primary magmatic and (retro)metamorphic minerals (metapelitic gneisses and pegmatoids mainly composed of quartz, K-feldspar, plagioclase, and biotite) have been extensively dissolved and replaced by clay mineral assemblage formed by intimately mechanically mixed illite and sudoite. The XRD patterns of air-dried oriented preparations of clay samples show the characteristic 001 reflections of sudoite at 14.07, 7.12, 4.74 and 3.54 Å, with a particularly intense 003 reflection (Fig. 2b). None of these 001 reflections is affected by ethylene-glycol solvation. Sudoite usually occurs as irregular staked flakes (Fig. 1f). In addition to the hydrothermal sudoite, pre-existing Fe-Mg trioctahedral chlorite inherited from the retrograde metamorphism that affected the basement before the deposition of the Athabasca Basin is found in increasing relative proportions with an increasing distance from the orebody.

The BET specific surface area of the rock samples from the strongly altered sandstone, the orebody and the altered basement is rather homogeneous over the investigated zone and ranges from 14 to 23 $\text{m}^2 \text{g}^{-1}$. Nitrogen adsorption isotherms are of type IIb with no saturation plateau and display H3 hysteresis loops according to the IUPAC classification. All these features are characteristic of a clay microporous structure. Pore size distributions of these samples are complex and are characterized by a sharp distribution of the micropores, with a maximum at 10 Å, and by a bimodal distribution in the mesopores range (between 20–40 and 60–100 Å).

4.2. Evolution of H_2 release upon thermal desorption of core samples

A total of 49 samples from different lithologies and different boreholes were selected for gas desorption experiments. Hydrogen was recovered by flow-through thermal desorption and quantified online by GC (Table 1). From the thermal desorption patterns of H_2 , the 49 samples can be divided into 3 groups. These 3 groups also correspond to the mineralogical zonation of the different alteration haloes described above.

The first group produces less than 5 ppm (g of H_2 per ton of rock) of H_2 upon heating to 300 °C. All these samples are located far from the deposit (i.e. more than 20 m from the orebody). Sam-

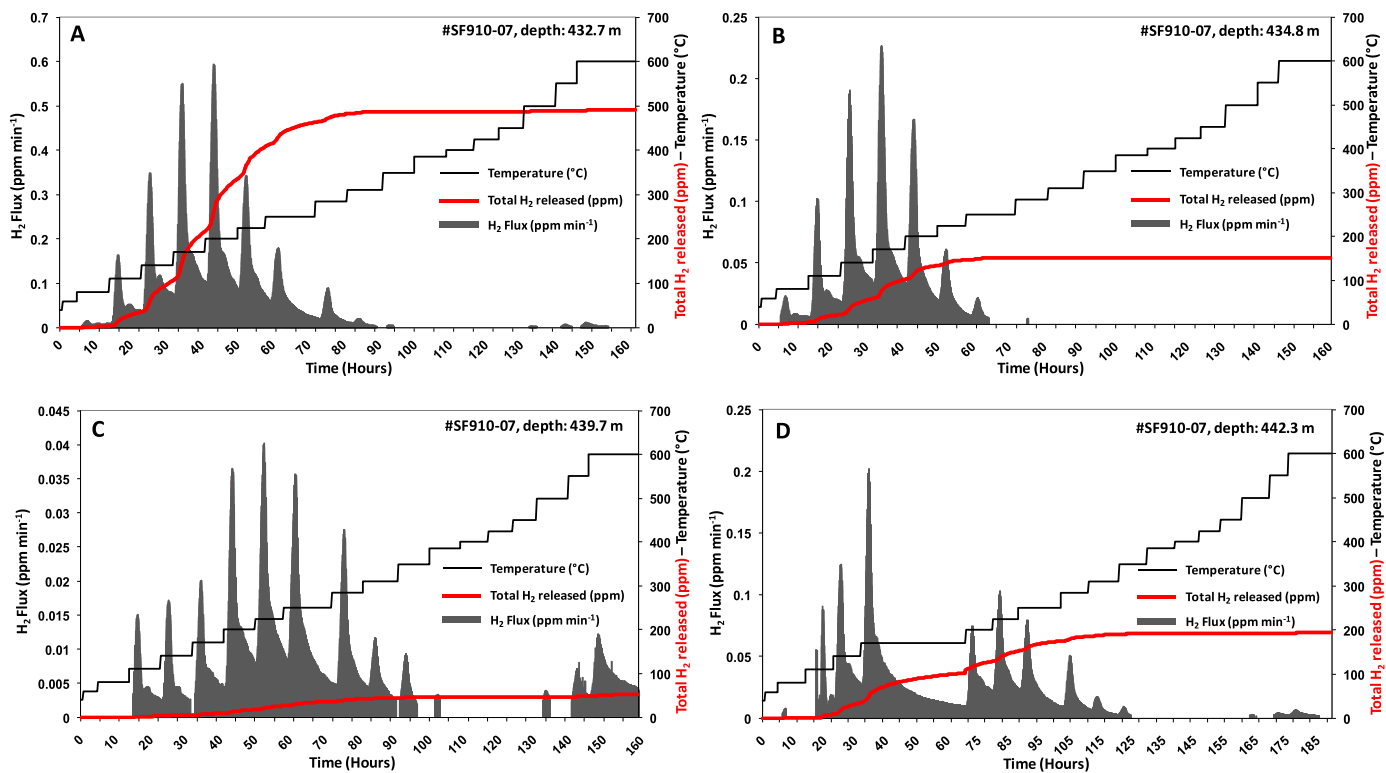


Fig. 3. Hydrogen (H_2) thermal desorption patterns (flux and total H_2 released) of four different core samples (borehole SF-910-07) from the Cigar Lake U deposit. Samples are located, in the ore zone at 432.7 m (A) and 434.8 m (B) depth, and in the clay altered basement below the deposit at 439.7 m (C) and 442.3 m (D) depth. H_2 concentration is given in ppm (g of H_2 per tons of rock). Hydrogen is fully released within minutes at each T step between 80 and 300 °C.

ples located above the deposit (i.e. in the strongly altered sandstones) contain illite, quartz and kaolinite. Samples located below the deposit (i.e. below the unconformity) contain illite, chlorite (mostly Al–Mg di-trioctahedral sudoite, and increasingly at depth Fe–Mg trioctahedral chlorite), and muscovite. Minor amount of CO_2 (less than 1000 ppm) is also produced at $T \geq 200$ °C, but CH_4 , CO and He are not detected.

The second group of samples releases 5 to 500 ppm of H_2 upon heating to 300 °C (Fig. 3). Hydrogen starts to be produced within minutes at 80 °C and is fully released at ~ 300 °C. Minor amount of H_2 may be also produced at $T \geq 400$ °C, but it represents less than 5% of the total amount of H_2 recorded. Over the 80–300 °C step-wise heating range, each stage is marked by a peak of hydrogen flux occurring few minutes after each T increment. The hydrogen desorption flux reaches a maximum at ~ 200 °C and then decreases progressively until complete exhaustion at 300–350 °C. All samples from this second group display this typical bell-shape peaks pattern of H_2 flux centered on 200 °C. Minor amounts of CO_2 (less than 1000 ppm), CH_4 (10 to 50 ppm) and He (up to 6 ppm) are also released at $T < 350$ °C. The richest H_2 -bearing samples are located in the ore zone and in the strongly argillized basement just below the mineralization (<20 m). They all contain illite and sudoite, but not necessarily uraninite. Indeed, the samples located in the basement are free of uranium (Fig. 6). Siderite is absent from all these samples. The δD of H_2 recovered during thermal desorption of these samples ranges from -582 to -517‰ with a mean value of -550‰ ($n = 5$, Table 1).

The third group concerns only two particular samples located just above the ore zone, in the narrow clay-rich hematitic zone. These two samples produce 331 and 1119 ppm of H_2 mostly at $T \geq 350$ °C (Fig. 4). Only 15 and 57 ppm of H_2 are released at $T < 350$ °C, respectively. The hydrogen flux displays several peaks over the 350–600 °C T range, but the shape of the pattern is completely different than the one recorded for the second group of

samples (i.e. no symmetry, strong peak overlaps). Huge amount of CO_2 (2.3 and 7.6 wt% for samples producing 331 and 1119 ppm H_2 , respectively) are also released at $T \geq 350$ °C. These two samples contain significant amount of hematite (11 and 6 wt%) and siderite (6 and 17 wt%, respectively) in addition to illite and kaolinite. The sample producing 331 ppm of H_2 exhibits a δD value of H_2 of -311‰ (Table 1).

Note that crushing, drying at 40 °C for 48 h, or storing the samples over several months under ambient condition does not induce any significant change in the amount of H_2 released. Total amounts of H_2 recovered by batch and flow-through desorption runs were similar.

Hydrogen concentration mapping at the scale of the deposit reveals a concentric zonation around the U orebody (Figs. 5a, 6). The common feature of all these H_2 -rich samples is their close relationship to the mineralization and their high clay content (from 70 to 100 wt%) dominated by illite and sudoite in the basement and the ore zone, and illite–hematite–siderite \pm kaolinite in the red alteration halo located just above the deposit (Fig. 5b).

5. Discussion

5.1. Source of H_2

It was found that grinding and drying the samples did not have significant effect on the amount of H_2 recovered in comparison with the run performed with undisturbed samples. This demonstrates that H_2 does not occur as a free gas phase in the intergranular porosity. Hydrogen production by autoclave corrosion, or by iron contamination during drilling can be excluded as demonstrated by the absence of hydrogen release in the core samples located far (>20 m) from the deposit. Thermal decomposition of trace of organic matter, if any, during desorption runs cannot account for the high H_2 concentration observed our samples. The

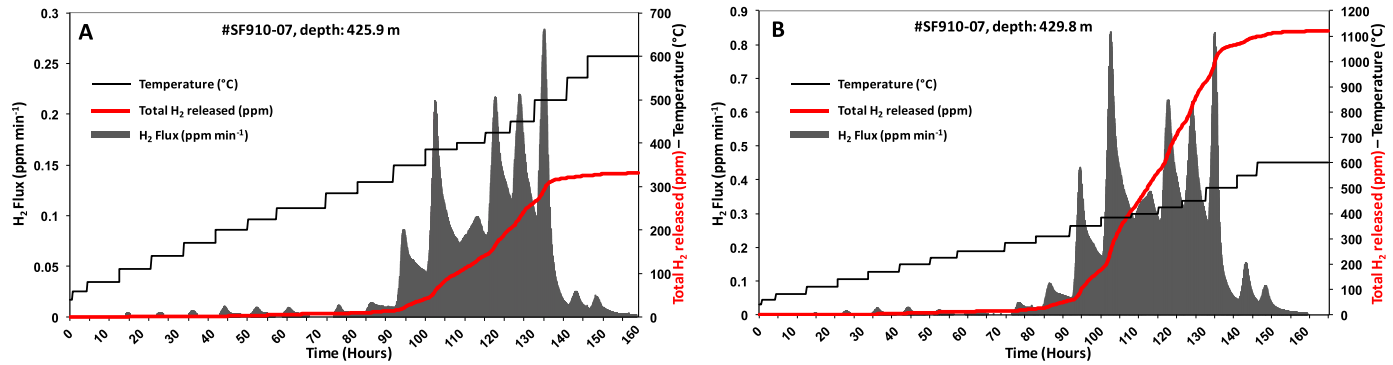


Fig. 4. Hydrogen (H_2) thermal desorption patterns (flux and total H_2 released) of two particular samples located in the clay-rich hematitic-siderite zone located just above the orebody at 425.9 m (A) and 429.9 m (B) depth. H_2 concentration is given in ppm (g of H_2 per tons of rock). In these two samples, and contrarily to the general behavior of hydrogen release upon thermal desorption shown in Fig. 3, H_2 is mostly produced at higher temperature, from 350 to 600 °C. Siderite hydrothermal alteration triggered by clay minerals deshydroxylation at $T > 350$ °C during the thermal desorption run explains this observation.

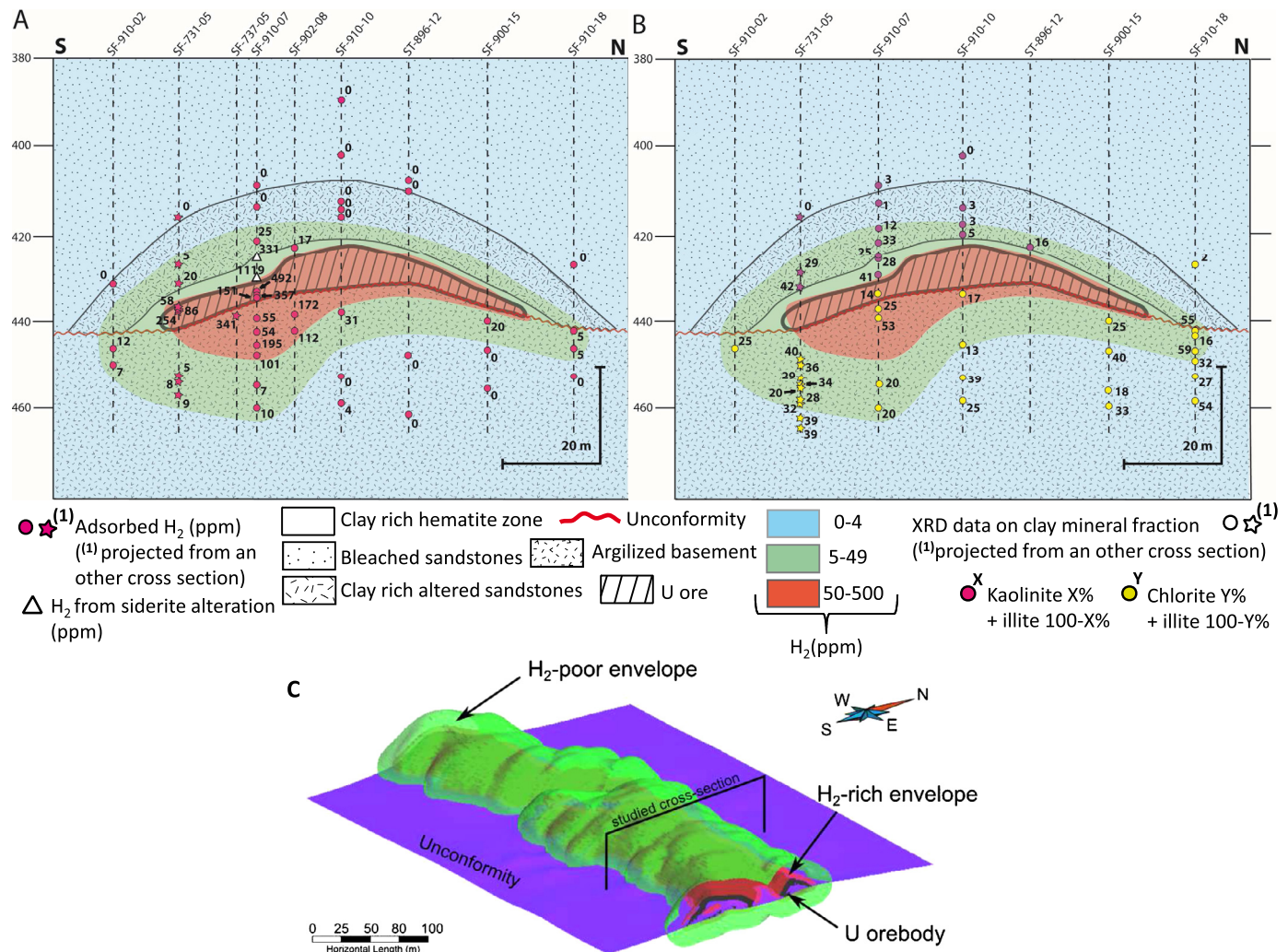


Fig. 5. North–South cross-section maps of (A) hydrogen concentration, and (B) clay mineralogy in the Cigar Lake uranium deposit. H_2 concentration is given in ppm (g of H_2 per tons of rock) along the path of the nine different boreholes (referenced as SF or ST above the figure – exact location reported in Table 1) alienated along this cross-section. The different lithologies are superimposed to the three different envelopes delineating the H_2 -rich ($[H_2] \geq 50$ ppm), the H_2 -poor ($5 \leq [H_2] < 50$ ppm) and the H_2 -free ($[H_2] < 5$ ppm) zones. (C) 3D view of the Cigar Lake uranium ore deposit obtained by geomodeling (Appendix A). The H_2 -rich and H_2 -poor surrounding envelops are underlined in light red and green colors, respectively.

total organic carbon content is less than 0.1 wt% in the argillized basement and ranges from <0.1 to 0.5 wt% in the strongly altered sandstones (Landais et al., 1993). The H/C atomic ratio of organic matter, when present, ranges between 0.7 and 0.8. Even a total pyrolysis of organic matter into graphite cannot explain the high

H_2 concentrations (up to 0.11 wt%) in our samples. Thus, the two other hydrogen sources that can be accounted for in the present case are: i) hydrogen artificially generated by hydrothermal reactions during samples heating, and ii) hydrogen entrapped by the clay-rich rocks in the close vicinity of the deposit and being re-

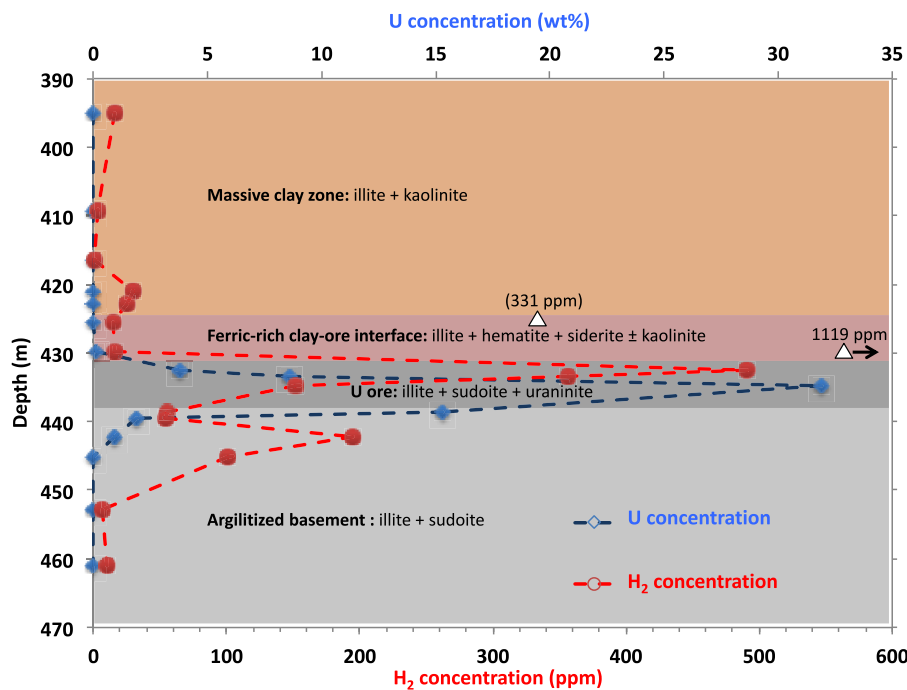


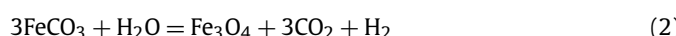
Fig. 6. Adsorbed hydrogen concentration (red circles) and whole rock uranium content (blue diamonds) as a function of depth along borehole SF-910-07. The red circles correspond to the amount of adsorbed hydrogen released in the 80–300 °C T range during the thermal desorption runs. Hydrogen concentration decreases gradually when moving away of the deposit, but there is no direct correlation with the uranium content of the ore. The highest concentrations of adsorbed H_2 are found in the ore zone and below in the sudoite-rich argilized basement. As an exception, hydrogen is mostly produced by siderite hydrothermal alteration at $T > 350$ °C (white triangles) in the clay-rich hematitic zone located just above the orebody.

leased by thermal desorption. These two hypotheses are discussed below.

5.1.1. Hydrogen generation by hydrothermal reactions during the runs

The core samples are naturally water saturated, and drying at 40 °C is not sufficient to ensure dehydration of clay minerals. Thus, artificial hydrogen generation induced by hydrothermal alteration/oxidation of Fe^{2+} -bearing minerals (i.e. siderite and $Fe\text{-Mg}$ chlorite) and U^{4+} -bearing minerals (uraninite, pitchblende) during the thermal desorption runs is feasible. Nevertheless, this eventuality can be ruled out in cases where H_2 is released at $T \leq 300$ °C (i.e. primarily samples from the ore zone and the basement) for the three following reasons. First, the amount of hydrogen produced is not correlated to the iron and uranium content of the rock. Some samples free of uraninite and/or of Fe^{2+} -bearing minerals are rich in H_2 . Second, the desorption flux of H_2 always exhibits the same pattern with ~7 distinct maxima over the stepwise heating range (Fig. 3). Such a behavior is hardly explainable by the potential occurrence of more than seven different H_2 -producing hydrothermal reactions each having their own activation energy. Third, hydrogen production occurs within few minutes at each T step in the 80–300 °C range. Such low temperatures, together with the very short resident time of water in the flow-through autoclave (water vapor is constantly removed by a constant Ar flux of 0.1 l min⁻¹) are not compatible with efficient and rapid hydrogen production through hydrothermal reactions (McCollom and Seewald, 2001; Mayhew et al., 2013; Milesi et al., 2015).

However, in the two samples where H_2 is released at $T \geq 350$ °C (i.e. samples from the very localized clay-rich hematitic-siderite zone; Figs. 4 and 5), H_2 may be produced by thermal decomposition of siderite in the presence of water vapor according to Eqn. (2) (McCollom, 2003; Milesi et al., 2015).



In these two latter samples, water does not originate from the initial pore saturation state as it was removed at the early stages of the heating ramp by the Ar flux, but it may be produced by dehydroxylation of clay minerals (illite and kaolinite) at $T \geq 350$ °C. The tv-1M and cv-1M illite varieties are described in the Cigar Lake hydrothermal alteration haloes (Percival et al., 1993; Drits et al., 1993). Cis-vacant 2:1 layers in illite start to dehydroxylate at $T \geq 600$ °C, but trans-vacant 2:1 layers dehydroxylate at much lower T , ranging from 350 to 600 °C (Drits et al., 1998). The dehydroxylation process of kaolinite starts at ~450 °C and peaks at 525 °C (Beaufort et al., 1998). The sequential dehydroxylation of illite and kaolinite explains the successive overlapping peaks of hydrogen flux over the 350–600 °C T range, and the two main bursts of H_2 recorded at 400 and 500 °C, respectively. Mass balance calculation based on Eqn. (2) confirms this hypothesis as the amount of CO_2 (0.53 and 1.7 mol kg⁻¹, respectively) is approximately three times higher than the amount of H_2 produced (0.16 and 0.56 mol kg⁻¹, respectively). The theoretical amount of siderite and water required to produce the measured amount of H_2 and CO_2 through thermal decomposition (Eqn. (2)) corresponds perfectly to the initial siderite content of the samples (as deduced by XRD) and to a complete dehydroxylation of the clay fraction. The δD of H_2 (~−311‰) produced by one sample belonging to this zone is also significantly different from that of the samples from the orebody and the argilized basement (mean value at ~−550‰). Hydrogen may be also produced in minor amount (<200 ppm) during dehydroxylation of clay minerals at $T > 400$ °C (Heller-Kallai et al., 1989; Villieras et al., 1992; Heide and Földvari, 2006). Nevertheless, dehydrogenation process in itself seems to be a minor contribution to H_2 generation in the Cigar Lake samples as demonstrated by the very limited H_2 released from clay-rich (illite + kaolinite or chlorite) samples free of siderite that are located far from the deposit (Figs. 5, 6). Hence, the elevated concentrations of H_2 (up to 0.11 wt%) and CO_2 (up to 7.6 wt%) recorded in the two samples from the narrow clay-rich

hematitic zone located just above the orebody correspond to hydrogen generation by siderite thermal decomposition triggered by illite and kaolinite dehydroxylation during the thermal desorption runs at $T \geq 350^\circ\text{C}$. This artificially induced hydrogen production is restricted to the thin siderite-bearing rim located just above the deposit. It represents an exception to the general behavior of H_2 upon thermal desorption, and is thus not accounted for in our subsequent calculation of H_2 uptake in the deposit.

5.1.2. Water radiolysis and hydrogen sorption on clay minerals

This process is the more relevant to explain the high hydrogen amounts (up to 500 ppm) released at $T < 350^\circ\text{C}$ in the ore-zone and in the argillized basement, but also, albeit in a lesser extent, in the altered sandstones above the orebody. Together, the hydrogen concentric zonation (Figs. 5a and 6) and isotopic signature ($\delta\text{D}_{\text{H}_2} = -550 \pm 30\text{\textperthousand}$), the release of He upon thermal desorption runs, and the presence of dissolved H_2 ($8.25 \times 10^{-4} \text{ mol l}^{-1}$) and He (up to $5.54 \times 10^{-5} \text{ mol l}^{-1}$) in the ground-water sampled within the orebody (Liu and Neretnieks, 1996; Bruno and Spahiu, 2014) confirm that water radiolysis sustained by the massive and focus U mineralization over the life-time of the deposit is the main source of H_2 . Calculations of H_2 production by water radiolysis reported below also support this conclusion (Appendix B). Furthermore, the rapid release of H_2 at T as low as 80°C , the sequential release of H_2 over the $80\text{--}300^\circ\text{C}$ stepwise heating range (Fig. 3), the very low organic matter content (<0.5 wt% if present), and the absence of correlation between hydrogen, iron and uranium contents in the rocks, clearly point to adsorption (physisorption) processes of H_2 on multiple binding sites at the surface of clay minerals massively present in the ore zone and its vicinity, and not to *in situ* generation of H_2 induced by hydrothermal or dehydrogenation processes during the thermal desorption runs as discussed above.

Our measurements cannot completely discard other potential natural hydrogen sources that may have contributed to the total amount of hydrogen recovered by thermal desorption, such as microbial H_2 production by anaerobes (Hoehler et al., 2001; Nealson et al., 2005), deep hydrogen migration channeled by the faults deeply rooted in the basement, or hydrothermal alteration of Fe^{2+} -bearing minerals during the deposit genesis. It is worth mentioning here that ultramafic or serpentized rocks are not reported in the Aphebian metasediment basement of the Athabasca basin (Jefferson et al., 2007). In any case, the above-mentioned arguments indicate that such contributions must have been minor in supplying hydrogen for sorption compare to water radiolysis.

5.2. Nature of the sorbent and H_2 sorption process

The nature of the minerals that trap H_2 in the ore-zone and in the basement (i.e. where hydrogen is released at $80 \leq T \leq 300^\circ\text{C}$) may be inferred from the comparison of both the mineralogy and the H_2 thermal desorption patterns of samples from these zones in one hand and samples from the hematitic zone and the altered sandstones located above the deposit in the other hand. All these samples contain illite (both cv-1M and tv-1M polytypes), but those located in the hematitic zone and above contain kaolinite instead of chlorite. These latter samples do not release significant amount of H_2 (<60 ppm) in the $80\text{--}300^\circ\text{C}$ T range despite their immediate proximity with the deposit (<20 m). This means that both illite and kaolinite do not sorb significant amount of hydrogen. Uraninite is not responsible for H_2 sorption because samples free of U located in the basement also contain significant amount of H_2 and display similar thermal desorption patterns (Figs. 3 and 6). The amount of organic matter in the deposit is insufficient to account for the high hydrogen uptake. Therefore, chlorite is the only mineral that explains both the hydrogen zonation and the

thermal desorption behavior of H_2 in the $80\text{--}300^\circ\text{C}$ T range. Al-Mg di-trioctahedral sudoite is very probably the chlorite variety responsible for much of the H_2 adsorbed in the deposit, as it is far more abundant than the Fe-Mg trioctahedral chlorite that appears mostly at depth in the argillized basement. The physicochemical characteristics of the illite-sudoite intergrowth and associated porous network may be also important in defining the adsorption properties within the pores of the rock.

Even if providing a definitive picture of H_2 sorption mechanism at the surface of clay minerals, and in particular chlorite, is beyond the scope of this study, some important considerations may be laid down. The absence of a permanent dipole moment, the small Van der Walls' radius (1.375 Å), and the high strength of the H-H σ -bond (436 kJ mol $^{-1}$) involving the only two valence electrons available make molecular hydrogen extremely mobile and poorly reactive. In the absence of charged sites, H_2 can only bind to surfaces through weak van der Waals' forces. However, hydrogen can bind to surfaces through induced dipole and enhanced quadrupole moments in the presence of an external potential (Kolos and Wolniewicz, 1967; Lochan and Head-Gordon, 2006). Therefore, the key requirements to induce hydrogen physisorption are a high surface area, and a high density of binding sites exposing H_2 to overlapping electrostatic fields (Edge, 2014). Creation of strong electrostatic fields within a cavity through a charged framework and counterions, and reduction of pore size toward the kinetic diameter of H_2 (2.9 Å) is the principle behind much research on intercalates, zeolites and metal-organic frameworks, seeking to improve the thermodynamic properties for H_2 adsorption (Dinca et al., 2006). The significance of H_2 's polarizability in strengthening the bond between H_2 and accessible alkali metal cations has been demonstrated both theoretically (Solans-Monfort et al., 2004) and experimentally (Dinca et al., 2006).

To our knowledge, hydrogen sorption mechanism on clays has only been studied for swelling 2:1 smectites: montmorillonite (Gil et al., 2009; Didier et al., 2012; Bardelli et al., 2004; Mondelli et al., 2015) and laponite (Edge, 2014; Edge et al., 2014). Neutron scattering has revealed the structure and dynamics of molecular H_2 physisorbed in the interlayer space of montmorillonite and laponite (Edge et al., 2014; Mondelli et al., 2015). Up to four hydrogen molecules coordinate directly to partially solvated interlayer cations. The transport of H_2 occurs via a jump diffusion mechanism leading to a H_2 diffusion coefficient an order of magnitude slower than in bulk liquid water. Volumetric measurements have shown that hydrogen uptake by a dehydrated outgassed Ca-laponite reaches 0.2 wt% at 77 K and 1 bar hydrogen partial pressure (Edge et al., 2014), the theoretical limiting uptake being around 0.82 wt% and corresponding to a complete monolayer of interlayer H_2 . High pressure volumetric measurements performed by Mondelli et al. (2015) on synthetic dry Na-montmorillonite at 90°C indicate that hydrogen adsorption saturates between 40 and 60 bar, reaching 0.2 wt% at the plateau. Direct comparison between these studies and the present one is difficult, because they cover different range of T and P , and different type of clays, but irrespective of the conditions, hydrogen concentration remains in the same range from a few hundred to a few thousand ppm. Nevertheless, all these pioneering studies performed on smectites suggest that water, a highly polar molecule, and hydrogen will undergo competitive adsorption.

Surprisingly, despite the fact that swelling clays are not present in the Cigar Lake deposit and that the media is fully water-saturated, the amount of hydrogen adsorbed is comparable with that measured on pure, dry, outgassed synthetic smectites. Kaolinite has no layer charge, thus does not attract interlayer cations and cannot provide cation bidding-sites for H_2 . Illite and chlorite show low CEC (0.1–0.4 meq g $^{-1}$), and the dry interlayer space is too small for a hydrogen molecule (Kameda et al., 2007). Thus,

hydrogen interaction mechanisms with chlorite, illite and kaolinite are certainly different than the one involved with smectite interlayer spaces. The adsorption of H₂ may occur in interlinked nanopores between clay particles, on the basal oxygen layers, and on the edge of the TOT sheets. The nanometer-scale pore networks are known to be a key controlling factor for gas (e.g. CH₄, CO₂) transfer in clay media (Aylmore, 1974; Aringhieri, 2004; Ross and Bustin, 2009). In micropores, the force fields of opposing pore walls are close enough that they will overlap and significantly influence adsorption behavior. Pores of few nanometers in diameters between crystal layers of clay particles are known to provide the adsorption sites for CH₄ and other gases due to the large surface area (Cheng and Huang, 2004). Such an eventuality has been probed both experimentally (Ji et al., 2012) and theoretically (Xiong et al., 2017) for methane adsorption on chlorite. Xiong et al. (2017), using grand canonical Monte Carlo simulations, reveal that methane is adsorbed on chlorite by physical adsorption and that the adsorption capacity in chlorite micropores (1 to 4 nm) is stronger than in mesopores (up to 20 nm). These approaches remain to be applied for hydrogen adsorption on chlorite, illite or kaolinite, but it is worth mentioning that hydrophobic materials like chlorite may decrease the competition between hydrogen and water to sorb on their surface. In non-swelling clays, the nature of the clay mineral layers that form the external basal surfaces of each particle can be different from the nature of the layers in the core of the particle. In addition, the location of the vacant sites (e.g. sudoite has octahedral vacancies), the presence of isomorphous substitution, and the absence of a few of the octahedral sheets between the 2:1 layers in the case of chlorite may profoundly influence the surface charge of the particles. The thermal desorption flux of H₂, displaying several well defined peaks over the 80–300 °C *T* range, reflects different binding energies and reveals a complex interplay between the different sorption sites (geometry and strength of the electrostatic forces surrounding the edges and basal surfaces, nature and texture of the mineral intergrowths) and the pore size distributions – pores having only a few H₂ diameters (~6–9 Å) being the more favorable for confining hydrogen adsorbate molecules.

5.3. Sorption processes affect hydrogen mobility in the crust

These surprisingly high hydrogen contents in clay-rich rocks challenge the fundamental assumption that hydrogen is not easily trapped in the Earth's crust (Smith et al., 2005). The interpretation of hydrogen behavior in the crust is based on a long-standing paradigm that if not consumed by bacterial activity at low *T* or abiogenic redox processes at high *T*, it diffuses through the rocks and escapes continually into the oceans or atmosphere. However, H₂ sorption processes are completely overlooked in our current models of hydrogen transfer in the crust (Sherwood Lollar et al., 2014; Worman et al., 2016). Clay minerals, and in the present case chlorite, are good candidates for H₂ physisorption. Besides their abundances, they display large accessible surface areas (~20 m² g⁻¹ for the rock samples investigated here), multiple binding sites surrounded by strong potential field, and pores or interlayer spaces of molecular dimensions of only a few H₂ diameters (~10 Å). On a global scale, sorption processes may represent a considerable uptake of H₂, and drastically affect the existing estimates of H₂ flux and distribution within continental and oceanic crust.

The hydrogen contents reported here in clay-rich rocks mostly constituted of illite and chlorite are in the same order of magnitude as methane adsorbed on shale, a clastic clay-rich sedimentary rock that is known for its potentially significant gas content. Shale gases are unconventional gas systems in which the shale is both the source of, and the reservoir for, methane (e.g. Ross

and Bustin, 2009). Methane, as well as hydrogen, is a non-polar molecule and a comparison between the adsorption properties of these two compounds on porous materials is meaningful. Organic matter is the main element which controls gas adsorption on shale gas reservoirs, but clay minerals play an important role too (Ross and Bustin, 2009; Zhang et al., 2012; Kuila et al., 2014). Ross and Bustin (2009) indicate that high pressure (60 bar) CH₄ sorption capacities at 30 °C under moisture equilibration condition range from 71 ppm (4.4×10^{-3} mol kg⁻¹) for organic lean shales to 1429 ppm (89.3×10^{-3} mol kg⁻¹) for organic rich shales. For comparison, the following CH₄ adsorption capacities are reported by Ji et al. (2012) for various dry clay minerals at 35 °C and about 60 bar of methane: 4500 ppm for montmorillonite, 1000 ppm for kaolinite and about 800 ppm for illite and chlorite. Note that the presence of water is also known to compete with methane on the sorption sites. At Cigar Lake, i) the rocks are fully water-saturated, ii) the total organic content is very low (<0.5 wt%), iii) the presence of other adsorbed gases (CO₂, CH₄, and He also released during the thermal desorption experiments; Table 1) may compete with H₂ on the sorption sites, and iv) the hydrogen partial pressure is probably around 1 bar assuming equilibrium with dissolved hydrogen concentration reported in the groundwater sampled in the ore ([H₂] = 8.25×10^{-4} mol l⁻¹ – Bruno and Spahiu, 2014). Despite these limiting parameters, hydrogen adsorption reaches the spectacular concentration of 500 ppm (i.e. 0.250 mol kg⁻¹). The clay-rich rocks from Cigar Lake deposit are probably not saturated with respect to hydrogen and higher H₂ contents are expected on pure, dried and outgassed clay fractions at higher H₂ partial pressure. Thus, it appears that hydrogen uptake by clay minerals is by no means negligible compare to methane, and may even exceed it.

In the example of Cigar Lake deposit, an estimate of the total amount of H₂ trapped in the rock can be calculated. Using an H₂-rich ([H₂] ≥ 50 ppm) rock tonnage of 1.84×10^6 tons at a mean H₂ content of 190 ppm (*n* = 13), and an H₂-poor (5 ≤ [H₂] < 50 ppm) rock tonnage of 8.46×10^6 ton at a mean H₂ content of 15 ppm (*n* = 15), we obtain an estimate of 476 tons of H₂ currently trapped in the deposit (see Appendix A for detailed calculation, and Fig. 5c). Note that the mean H₂ content of each envelop is calculated taking into account only the samples that release H₂ at $80 \leq T \leq 300$ °C, i.e. where sorption is demonstrated. The two samples from the narrow hematitic-siderite clay-rich zone were discarded from these calculations. The estimated amount of H₂ trapped in the deposit has to be compared with theoretical calculation of hydrogen production by water radiolysis. For an orebody of grade 14 wt% U and 10% porosity, the maximum hydrogen production rate by water radiolysis per kilogram of U is 1.97×10^{-15} mol s⁻¹ kg⁻¹ (see Appendix B for detailed calculation). When integrated over the 1.4-Ga-lifetime of the deposit, and given the estimated U tonnage 82,600 tons, this yields a maximum H₂ production of 1.34×10^4 tons. This conservative (maximum) estimate of the hydrogen production by water radiolysis compared to the actual hydrogen content in the deposit indicates that at least ~4% of the produced H₂ have been trapped in the clay alteration halo surrounding the deposit. This estimation even reaches 17% if we consider that the entire ore deposit has been affected by late remobilizing events 300 Ma ago (Fayek et al., 2002). In addition, the efficiency of radiolysis (the real H₂ production rate over the maximum possible H₂ production rate) is probably lower than calculated because hydrogen produced by water radiolysis is largely scavenged by the oxidants (O₂, H₂O₂) generated in the same process and by bacterial activity (Bruno and Spahiu, 2014).

6. Conclusions

This work reveals for the first time that hydrogen is adsorbed at the surface of water-saturated clay minerals present in sedi-

mentary and basement rocks. Up to 500 ppm H₂ were released within minutes during stepwise thermal desorption (80–300 °C) of the clay-rich rocks (mainly composed of illite and sudoite) present in the orebody and the argilitized basement of the Cigar Lake uranium deposit. These surprisingly high hydrogen amounts shift the long-standing paradigm that H₂ is extremely mobile and cannot be stored within the lithosphere.

Sudoite, a Al–Mg di-trioctahedral chlorite, is probably the mineral that sorbs most of hydrogen in this context, even if a contribution of illite or Fe–Mg tri-octahedral chlorite cannot be discarded. The properties of the micropore network and the variety of the binding sites may play a key role in promoting hydrogen sorption.

Hydrogen adsorption at the surface of clay minerals must be considered seriously as it may drastically impact H₂ fate and mobility in various geological contexts where large amounts of hydrogen are produced (e.g. serpentinized ultramafic rocks, fracture networks in crystalline rocks, peralkaline igneous complexes). Even if this study must now be extended to other geological settings, the potential for clay-rich rocks to trap hydrogen may represent a new unexpected target for energy exploration and storage.

Acknowledgements

The authors acknowledge Orano group for financial support. Orano Mining BU and Cameco are also thanked for providing the samples and scientific collaboration. Many thanks to H. Toubon, P. Ledru, M. Brouand and P. Nardoux, who contributed greatly in making this work feasible. We thank V. Magnin for BET measurements and E. Bazarkina, L. Charlet and B. Lanson for inspiring scientific discussions. The article benefited from comments of the editor M. Bickle and two anonymous reviewers.

Appendix. Supplementary material

The supplementary material contains two pdf files that are cited in the main text as Appendix A (Calculation of the volume of the H₂-rich and H₂-poor envelopes), and Appendix B (Calculation of the radiolytic H₂ yield).

Supplementary material related to this article can be found online at <https://doi.org/10.1016/j.epsl.2018.04.038>.

References

- Aringhieri, R., 2004. Nanoporosity characteristics of some natural clay minerals and soils. *Clays Clay Miner.* 52, 700–704.
- Aylmore, L.A.G., 1974. Gas sorption in clay mineral systems. *Clays Clay Miner.* 22, 175–183.
- Bardelli, F., Mondelli, C., Didier, M., Vitillo, J.G., Cavicchia, D.R., Robinet, J.-C., Charlet, L., 2004. Hydrogen uptake and diffusion in Callovian-Oxfordian clay rock for nuclear waste disposal technology. *Appl. Geochem.* 49, 168–177.
- Beaufort, D., Cassagnabère, S., Petit, S., Lanson, B., Berger, G., Lachapagne, J.C., Johansen, H., 1998. Kaolinite-to-dickite reaction in sandstone reservoirs. *Clay Miner.* 33, 297–316.
- Billault, V., Beaufort, D., Patrier, P., Petit, S., 2002. Crystal chemistry of Fe-sudoite from uranium deposits in the Athabasca Basin (Saskatchewan, Canada). *Clays Clay Miner.* 50, 70–81.
- Bruneton, P., 1993. Geological environment of the Cigar Lake uranium deposit. *Can. J. Earth Sci.* 30, 653–673.
- Bruno, J., Spahiu, K., 2014. The long-term effect of hydrogen on the UO₂ spent fuel stability under anoxic conditions: findings from the Cigar Lake natural analogue study. *Appl. Geochem.* 49, 178–183.
- Cannat, M., Fontaine, F., Escartin, J., 2010. Serpentinization and associated hydrogen and methane fluxes at slow spreading ridges. In: Diversity of Hydrothermal Systems on Slow Spreading Ocean Ridges, pp. 241–264.
- Charlou, J.L., Donval, J.P., Fouquet, Y., Jean-Baptiste, P., Holm, N.G., 2002. Geochemistry of high H₂ and CH₄ vent fluids issuing from ultramafic rocks at the Rainbow hydrothermal field (36°14'N, MAR). *Chem. Geol.* 191, 345–359.
- Cheng, A.I., Huang, W.L., 2004. Selective adsorption of hydrocarbon gases on clays and organic matter. *Org. Geochem.* 35, 413–423.
- Didier, M., Leone, L., Grenache, J.-M., Giffaut, E., Charlet, L., 2012. Adsorption of hydrogen gas and redox processes in clays. *Environ. Sci. Technol.* 46, 3574–3579.
- Dinca, M., Dally, A., Liu, Y., Brown, C.M., Neumann, D.A., Long, J.R., 2006. Hydrogen storage in a microporous metal-organic framework with exposed Mn²⁺ coordination sites. *J. Am. Chem. Soc.* 128, 16,876–16,883.
- Drits, V.A., Weber, F., Salyn, A.L., Tsipursky, S.I., 1993. X-ray identification of one-layer illite varieties: application to the study of illites around uranium deposits of Canada. *Clays Clay Miner.* 41, 389.
- Drits, V.A., Lindgreen, H., Salyn, A.L., Ylagan, R.F., McCarty, D.K., 1998. Semiquantitative determination of trans-vacant and cis-vacant 2:1 layers in illites and illite-smectites by thermal analysis and X-ray diffraction. *Am. Mineral.* 83, 1188–1198.
- Dubessy, J., Pagel, M., Beny, J.M., Christensen, H., Hickel, B., Kosztolanyi, C., Poty, B., 1988. Radiolysis evidenced by H₂-O₂ and H₂-bearing fluid inclusions in three uranium deposits. *Geochim. Cosmochim. Acta* 52, 1155–1167.
- Edge, J., 2014. Hydrogen Adsorption and Dynamics in Clay Materials. PhD thesis. University College London.
- Edge, J.S., Skipper, N.T., Fernandez-Alonso, F., Lovell, A., Srinivas, G., Bennington, S.M., Youngs, T.G., 2014. Structure and dynamics of molecular hydrogen in the interlayer pores of a swelling 2:1 clay by neutron scattering. *J. Phys. Chem. C* 118, 25,740–25,747.
- Fayek, M., Harrison, T.M., Ewing, R.C., Grove, M., Coath, C.D., 2002. O and Pb isotopic analyses of uranium minerals by ion microprobe and U–Pb ages from the Cigar Lake deposit. *Chem. Geol.* 185, 205–225.
- Gil, A., Trujillano, R., Vicente, M.A., Korili, S.A., 2009. Hydrogen adsorption by microporous materials based on alumina-pillared clays. *Int. J. Hydrg. Energy* 34, 8611–8615.
- Heide, K., Földvari, M., 2006. High temperature mass spectrometric gas-release studies of kaolinite Al₂[Si₂O₅(OH)₄] decomposition. *Thermochim. Acta* 446, 106–112.
- Heller-Kallai, L., Milosavljević, I., Grayevsky, A., 1989. Evolution of hydrogen on dehydroxylation of clay minerals. *Am. Mineral.* 74, 818–820.
- Hoehler, T.M., Bebout, B.M., Des Marais, D.J., 2001. The role of microbial mats in the production of reduced gases on the early Earth. *Nature* 412, 324–327.
- Horita, J., Berndt, M.E., 1999. Abiogenic methane formation and isotopic fractionation under hydrothermal conditions. *Science* 285, 1055–1057.
- Huber, R., Langworthy, T.A., König, H., Thomm, M., Woese, C.R., Sleytr, U.B., Stetter, K.O., 1986. Thermotoga maritima sp. nov. represents a new genus of unique extremely thermophilic eubacteria growing up to 90 °C. *Arch. Microbiol.* 144, 324–333.
- Jefferson, C.W., Thomas, D.J., Gandhi, S.S., Ramaekers, P., Delaney, G., Brisbin, D., Cutts, C., Quirt, D., Portella, P., Olson, R.A., 2007. Unconformity-associated uranium deposits of the Athabasca Basin, Saskatchewan and Alberta. In: Goodfellow, W.D. (Ed.), *Mineral Deposits of Canada: A Synthesis of Major Deposit-Types, District Metallogeny, the Evolution of Geological Provinces, and Exploration Methods*. Special Publication no. 5. Geological Association of Canada, Mineral Deposits Division, pp. 273–305.
- Ji, L., Zhang, T., Milliken, K.L., Qu, J., Zhang, X., 2012. Experimental investigation of main controls to methane adsorption in clay-rich rocks. *Appl. Geochem.* 27, 2533–2545.
- Kameda, J., Miyawaki, R., Kitagawa, R., Kogure, T., 2007. XRD and HRTEM analyses of stacking structures in sudoite, di-trioctahedral chlorite. *Am. Mineral.* 92, 1586–1592.
- Kolos, W., Wolniewicz, L., 1967. Polarizability of the hydrogen molecule. *J. Chem. Phys.* 44, 1426–1432.
- Kuila, U., McCarty, D.K., Derkowska, A., Fischer, T.B., Topór, T., Prasad, M., 2014. Nano-scale texture and porosity of organic matter and clay minerals in organic-rich mudrocks. *Fuel* 135, 359–373.
- Landais, P., Dubessy, J., Derepue, J.M., Philp, R.P., 1993. Characterization of graphite alteration and bitumen genesis in the Cigar Lake deposit (Saskatchewan, Canada). *Can. J. Earth Sci.* 30, 743–753.
- Lin, L.-H., Slater, G.F., Sherwood Lollar, B., Lacrampe-Couloume, G., Onstott, T.C., 2005. The yield and isotopic composition of radiolytic H₂, a potential energy source for the deep subsurface biosphere. *Geochim. Cosmochim. Acta* 69, 93–903.
- Liu, J., Neretnieks, I., 1996. A model for radiation energy deposition in natural uranium-bearing systems and its consequences to water radiolysis. *J. Nucl. Mater.* 231, 103–112.
- Lochan, R.C., Head-Gordon, M., 2006. Computational studies of molecular hydrogen binding affinities: the role of dispersion forces, electrostatics, and orbital interactions. *Phys. Chem. Chem. Phys.* 8, 1357–1370.
- Mayhew, L.E., Ellison, E.T., McCollom, T.M., Trainor, T.P., Templeton, A.S., 2013. Hydrogen generation from low-temperature water–rock reactions. *Nat. Geosci.* 6, 478–484.
- McCollom, T.M., Seewald, J.S., 2001. A reassessment of the potential for reduction of dissolved CO₂ to hydrocarbons during serpentinization of olivine. *Geochim. Cosmochim. Acta* 65, 3769–3778.
- McCollom, T.M., 2003. Formation of meteorite hydrocarbons from thermal decomposition of siderite (FeCO₃). *Geochim. Cosmochim. Acta* 67, 311–317.
- Milesi, V., Guyot, F., Brunet, F., Richard, L., Recham, N., Benedetti, M., Prinzhofer, A., 2015. Formation of CO₂, H₂ and condensed carbon from siderite dissolution in the 200–300 °C range and at 50 MPa. *Geochim. Cosmochim. Acta* 154, 201–211.

- Mondelli, C.C., Vitillo, J.G., Didier, M., Brendle, J., Cavicchia, D.R., Robinet, J.C., Charlet, L., 2015. Hydrogen adsorption and diffusion in synthetic Na-montmorillonites at high pressures and temperature. *Int. J. Hydrol. Energy* 40, 2698–2709.
- Neal, C., Stanger, G., 1983. Hydrogen generation from mantle source rocks in Oman. *Earth Planet. Sci. Lett.* 66, 315–320.
- Nealson, K.H., Inagaki, F., Takai, K., 2005. Hydrogen-driven subsurface lithoautotrophic microbial ecosystems (SLiMEs): do they exist and why should we care? *Trends Microbiol.* 13, 405–410.
- Percival, J.B., Kodama, H., 1989. Sudoite from Cigar Lake, Saskatchewan. *Can. Mineral.* 27, 633–641.
- Percival, J.B., Bell, K., Torrance, J.K., 1993. Clay mineralogy and isotope geochemistry of the alteration halo at the Cigar Lake uranium deposit. *Can. J. Earth Sci.* 30, 689–704.
- Potter, J., Salvi, S., Longstaffe, F.J., 2013. Abiogenic hydrocarbon isotopic signatures in granitic rocks: identifying pathways of formation. *Lithos* 182, 114–124.
- Proskurowski, G., Lilley, M.D., Seewald, J.S., Früh-Green, G.L., Olson, E.J., Lupton, J.E., Sylva, S.P., Kelley, D.S., 2008. Abiogenic hydrocarbon production at Lost City hydrothermal field. *Science* 319, 604–607.
- Ross, D.J.K., Bustin, R.M., 2009. The importance of shale composition and pore structure upon gas storage potential of shale gas reservoirs. *Mar. Pet. Geol.* 26, 916–927.
- Scott Bishop, C., Mainville, A.G., Yesnik, L.D., 2016. Cigar Lake Operation Northern Saskatchewan, Canada. Cameco National Instrument 43-101, Open-File Report, 164 pp.
- Sherwood Lollar, B., Voglesonger, K., Lin, L.-H., Lacrampe-Couloume, G., Telling, J., Abrajano, T.A., Onstott, T.C., Pratt, L.M., 2007. Hydrogeologic controls on episodic H₂ release from Precambrian fractured rocks – energy for deep subsurface life on Earth and Mars. *Astrobiology* 7, 971–986.
- Sherwood Lollar, B., Onstott, T.C., Lacrampe-Couloume, G., Ballentine, C.J., 2014. The contribution of the Precambrian continental lithosphere to global H₂ production. *Nature* 516, 379–382.
- Smith, N.J.P., Shepherd, T.J., Styles, M.T., Williams, G.M., 2005. Hydrogen exploration: a review of global hydrogen accumulations and implications for prospectives area in NW Europe. In: Doré, A.G., Vining, B.A. (Eds.), *Petroleum Geology: Northwest Europe and Global Perspectives – Proceedings of the 6th Petroleum Geology Conference*, pp. 349–358.
- Solans-Monfort, X., Sodupe, M., Zicovich-Wilson, C.M., Gribov, E., Spoto, G., Busco, C., Ugliengo, P., 2004. Can Cu⁺-exchanged zeolites store molecular hydrogen? An ab-initio periodic study compared with low-temperature FTIR. *J. Phys. Chem. B* 108, 8278–8286.
- Truche, L., Berger, G., Destrieville, C., Pages, A., Guillaume, D., Giffaut, E., Jacquot, E., 2009. Experimental reduction of aqueous sulphate by hydrogen under hydrothermal condition: implication for the nuclear waste storage. *Geochim. Cosmochim. Acta* 73, 4824–4835.
- Villieras, F., Yvon, J., Cases, J.-M., Zimmermann, J.-L., Baeza, R., 1992. Dosage et localisation du fer II dans le talc et la chlorite par analyse spectrométrique des gaz de thermolyse. *C. R. Acad. Sci. Paris* 315, 1201–1206.
- Worman, S.L., Pratson, L.F., Karson, J.A., Klein, E.M., 2016. Global rate and distribution of H₂ gas produced by serpentinization within oceanic lithosphere. *Geophys. Res. Lett.* 43, 6435–6443.
- Xiong, J., Liu, X.J., Liang, L.X., Zeng, Q., 2017. Investigation of methane adsorption on chlorite by grand canonical Monte Carlo simulations. *Pet. Sci.* 14, 37–49.
- Zhang, T., Ellis, G.S., Ruppel, S.C., Milliken, K., Yang, R., 2012. Effect of organic-matter type and thermal maturity on methane adsorption in shale-gas systems. *Org. Geochem.* 47, 120–131.